Journal of Power Sources 185 (2008) 691–697

Contents lists available at ScienceDirect

Journal of Power Sources

journal homepage: www.elsevier.com/locate/jpowsour

Investigation on scandium-doped manganate $La_{0.8}Sr_{0.2}Mn_{1-x}Sc_xO_{3-\delta}$ cathode for intermediate temperaturesolid oxide fuel cells

Xiangling Yue[a,b], Aiyu Yan[a,b], Min Zhang[a,b], Lin Liu[a], Yonglai Dong[a], Mojie Cheng[a,*]

[a] Dalian Institute of Chemical Physics, Chinese Academy of Sciences, 457 Zhongshan Road, Dalian 116023, PR China
[b] Graduate School of the Chinese Academy of Sciences, Beijing 100049, PR China

ARTICLE INFO

Article history:
Received 21 June 2008
Received in revised form 4 August 2008
Accepted 20 August 2008
Available online 26 August 2008

Keywords:
$La_{0.8}Sr_{0.2}Mn_{1-x}Sc_xO_{3-\delta}$
Oxygen anionic vacancy
Composite cathode
Solid oxide fuel cells

ABSTRACT

Scandium-doped lanthanum strontium manganate $La_{0.8}Sr_{0.2}Mn_{1-x}Sc_xO_{3-\delta}$ (LSMS) combined with YSZ as composite cathode for anode-supported solid oxide fuel cell is investigated. The LSMS powders are prepared using the modified Pechini method. The XRD and H_2-TPR results reveal that non-stoichiometric defects are introduced into the perovskite lattice of LSMS samples as a result of Sc substitution, which leads to increased oxygen ion mobility in the Sc containing samples. But high level doping of Sc may results in the segregation of the Sc_2O_3 secondary phase at elevated temperature. The cells with the LSMS-containing cathodes exhibit higher performances, especially at lower temperatures, which can be ascribed to the increased oxygen anionic vacancies in the LSMS.

1. Introduction

Extensive attention has been paid to the research and development of intermediate temperature solid oxide fuel cells (IT-SOFCs, operated at 650–800 °C) in recent years, basically because of the various advantages brought by the reduced-temperature operation [1], including higher system stability, wider materials selectivity, and increased potential for cost-effective fabrications. With the development of anode supported IT-SOFCs, a thin layer of YSZ (8 mol% yttria-stabilized zirconia) electrolyte film with a thickness of about 10 μm can be employed, reducing the ohmic resistance to a negligibly small degree and thus making the reduced-temperature operation feasible [2]. For anode supported IT-SOFC, however, the overpotential from O_2 reduction reaction on the traditional cathode material has been found to be significantly high, which undoubtedly obstructs further enhancement of the cell performance.

Perovskite-type oxide $La_{1-x}Sr_xMnO_3$ (LSM) is conventionally considered as cathode material for IT-SOFCs based on YSZ electrolyte, chiefly due to its sufficiently high electronic conductivity, preferable chemical and thermal compatibility with YSZ. Using a composite cathode comprising LSM and YSZ [2–5], the single cell showed profoundly improved performance as a result of the enlarged cathode/electrolyte/gas triple phase boundaries (TPBs) where the electrochemical reactions mainly occurred. Nevertheless, the LSM–YSZ composite cathode can only attain superior performance at temperature above 800 °C; at temperature below 750 °C, it would suffer from a severe performance degradation [6].

Since the serious performance attenuation of the LSM–YSZ composite cathode at lower temperatures is primarily derived from the inadequate ion transport and oxygen reduction activity within the cathode, comprehensive efforts have been focused on improving the ion conductivity of the composite cathode. By introducing a ceria interlayer between YSZ electrolyte and the composite cathode [7] or by replacing YSZ with ceria to form LSM–ceria composite cathode [8], the cathode performance has been greatly promoted, ascribed to the increased oxygen ion mobility in the composite cathode which, thereby, abated the cathode polarization resistance (R_p). Furthermore, by adding $La_{0.4}Ce_{0.6}O_{1.8}$ (LDC) into LSM–YSZ composite cathode, a remarkable improvement in the cathode performance was achieved in our group recently [9].

Besides the structural modification of LSM–YSZ composite cathode, a great deal of attention has also been paid to the modification of LSM material, based on the fact that LSM has negligibly small oxygen ion conductivity (10^{-7} S cm^{-1} at 900 °C [10]) and that LSM displays low electrochemical activity towards O_2 reduction at reduced temperature. Substantive efforts concerning LSM modification have been carried out on multiple substitutions at catalytically active B sites in LSM [11–15]. By introducing aliovalent transition metal cations into the B sites of perovskite lattice, the oxide ion mobility of LSM material would be increased due to the synergistic valence variations and non-stoichiometric defects

* Corresponding author. Tel.: +86 411 84379049; fax: +86 411 84379049.
E-mail address: mjcheng@dicp.ac.cn (M. Cheng).

0378-7753/$ – see front matter © 2008 Elsevier B.V. All rights reserved.
doi:10.1016/j.jpowsour.2008.08.038

induced into the lattice. It has been reported that the lanthanum scandate is a mixed conductor with predominant oxide ion conduction at a wide range of P_{O_2}, and the high polarisability of Sc ion would make it easier for the oxide ion to transport though the lattice [16–18]. From this point of view, Sc seems to be a promising dopant to increase the ion conductivity of LSM materials. However, Sc^{3+} doping at B-site of LSM has rarely been covered in literature.

Here, we explore the substitution of Mn with Sc for LSM in our attempt to improve the performance of LSM-based cathode materials for IT-SOFC. The effect of the incorporation of Sc on the microstructure and the reducibility of LSM material, as well as the potential use of Sc substituted LSM perovskite as cathode material for IT-SOFC have been investigated.

2. Experimental

2.1. Material synthesis and characterization

The $La_{0.8}Sr_{0.2}Mn_{1-x}Sc_xO_{3\pm\delta}$ material was prepared by the modified Pechini method. La_2O_3 (A.R. 99.99%), $Sr(NO_3)_2$ (A.R. 99.5%), $Mn(NO_3)_2$ aqueous solution (A.R. 49–51%), $Sc(NO_3)_3{\cdot}6H_2O$ (A.R. 99.95%) were used as initial materials. La_2O_3 was dissolved in nitric acid, then the corresponding metal nitrate solutions were mixed in a stoichiometric molar ratio of $La_{0.8}Sr_{0.2}Mn_{1-x}Sc_xO_{3\pm\delta}$ (abbreviated as $LSMS_x$) with $x = 0$, 2, 5, and 10 mol%, respectively. The ammonium citrate tri-basic ($C_6H_{17}N_3O_7$) was then added in a 1:1 molar ratio regarding the total amount of cations. The resulting solution was continuously stirred under a certain pH and heating, yielding a viscous clear solution of metal–citrate complexes which was then heated, giving birth to a solid amorphous precursor. The precursor powders were calcined later at 900–1100 °C to form pure perovskite phase and suitable particle size distribution.

The phases present in the as-prepared powders were characterized by X-ray diffraction analysis (XRD), in a Rigaku miniflex diffractometer using Ni-filtered Cu Kα radiation, at a scan rate of 0.02° per second between 20° and 80°.

2.2. H_2 temperature-programmed reduction (H_2-TPR) test

Each sample was pressed, crushed and sieved to a size of 80–110 mesh for the H_2-TPR measurement, which were conducted on a fixed-bed continuous flow reactor. 50 mg sample was used for each test. The sample was firstly purged with a highly pure helium stream (≥99.999 vol.%) at a flow rate of 30 ml min^{-1} at 30 °C for 30 min during which the baseline became level. Then, the sample was flushed with an H_2/Ar (10 vol.% H_2 in argon, 50 ml min^{-1}) gaseous mixture for starting H_2-TPR measurement, which was performed from 30 to 950 °C with a heating rate of 10 °C min^{-1}. A thermal conductivity detector (TCD) was adopted to monitor the changes of hydrogen-signal, and the profile was automatically recorded with a computer from 100 to 950 °C.

2.3. Cell fabrication and evaluation

NiO and YSZ were used to prepare Ni/YSZ substrates. Anode-electrolyte substrates, comprising of a solid weight ratio of 40:60 NiO/YSZ, were produced via a standard organic tape-casting and colloidal suspension coating procedures, and co-sintered at 1400 °C for 2 h. The post-sintered anode/electrolyte assemblies were ca. 21 mm in diameter and 0.5 mm in thickness. The sintered thickness of the YSZ electrolyte film was ca. 15 μm.

$LSMS_x$ and YSZ in a weight ratio of 50:50 were used to prepare the composite cathodes. The mixtures of $LSMS_x$ and YSZ were ground thoroughly in ethanol for 0.5 h, after dried, a certain amount of organic binders and *n*-butanol solvent were added to form cathode pastes. The $LSMS_x$–YSZ composite cathodes were coated on the electrolyte surface and typically fired at 1100 °C for 2 h in air. The cathode as-prepared had an effective area of about 0.5 cm^2 and a thickness of about 30–40 μm.

The single cell performance evaluation was carried out on a homemade setup. Ag was adopted as current collector. The current–voltage (*I*–*V*) data were recorded from 800 to 650 °C at an interval of 50 °C. Hydrogen, bubbling through water at room temperature was fed to the anode as fuel gas and pure O_2 was fed to the cathode side as oxidant gas. Both gases were kept at a constant flow rate of 100 ml min^{-1}.

A Solartron electrochemical system including a 1287 potentiostat and a 1260 frequency response analyzer, interfaced to a computer, allowed the electrochemical impedance spectroscopy (EIS) measurements under open circuit conditions. The frequency ranged from 100 KHz to 0.1 Hz with signal amplitude of 10 mV.

3. Results and discussion

3.1. Structure analysis

The XRD patterns of $LSMS_x$ samples calcined at different temperatures are shown in Fig. 1. It can be detected that at a minor Sc concentration, Sc^{3+} incorporate into the perovskite lattice without forming impurities, whereas at a higher Sc concentration, Sc_2O_3 secondary phase tends to precipitate from perovskite lattice. In light of literatures [19–21], a great variety of metal ions could be introduced into the acceptor-doped perovskite structure like LSM provided that their ionic radii fit the sizes of the 12 coordinated A and octahedral B sites, e.g., $r_A > 0.90$ Å and $r_B > 0.51$ Å. Therefore, the Sc^{3+} should be accommodated in B-site of LSM crystal theoretically taking into account that Sc^{3+} has a radius of 0.745 Å. The XRD analysis demonstrate on the one hand, Sc can be doped into the B-site of LSM at minor contents, on the other hand, large degrees of Sc doping result in the precipitation of Sc_2O_3 phase since Sc^{3+} is significantly larger than Mn^{3+} (0.645 Å) and/or Mn^{4+} (0.53 Å).

The structure of $LSMS_x$ samples appears sensitive to the sintering temperature and doping concentration. From Fig. 1a and b, it can be observed that the peak at $2\theta = 31.6°$ corresponding to Sc_2O_3 phase becomes evident at higher temperature and Sc content, suggesting that the amount of Sc_2O_3 come out from the perovskite lattice increases with sintering temperature and Sc concentration. These phenomena can be interpreted by the variation of Goldschmidt tolerance factor *t*, which is strongly correlated with the stability of perovskite structure [22]. The tolerance factor can be obtained from ionic radii as $t = (r_A + r_O)/\sqrt{2}(r_B + r_O)$, in which r_A, r_B and r_O stand for the radius of A-site, B-site cations and oxygen ion, respectively. According to the above definition, the *t*-value decreases with increasing degree of relatively big Sc ion doping into LSM, indicating that the stability of the perovskite phase decreases with the increase of Sc concentration. Furthermore, it has been reported that the thermodynamic stability of perovskite phase increases with increasing Goldschmidt tolerance factor *t* [22,23]. The above correlations rationally explain the formation of Sc_2O_3 secondary phase at elevated temperature and doping content.

Compared with the LSM sample, it can also be seen that all peaks of LSMS samples have shifts in 2θ values, and this trends become apparent at higher Sc concentration (10 mol%) irrespective of the precipitation of Sc_2O_3. In Table 1, the positions of the strongest peaks, the *d* values corresponding to the strongest peaks, and the mean particle sizes estimated by means of the Scherrer equation are listed. Both the *d* values and the mean particle sizes vary with Sc concentration, which is possibly ascribed to the introduction

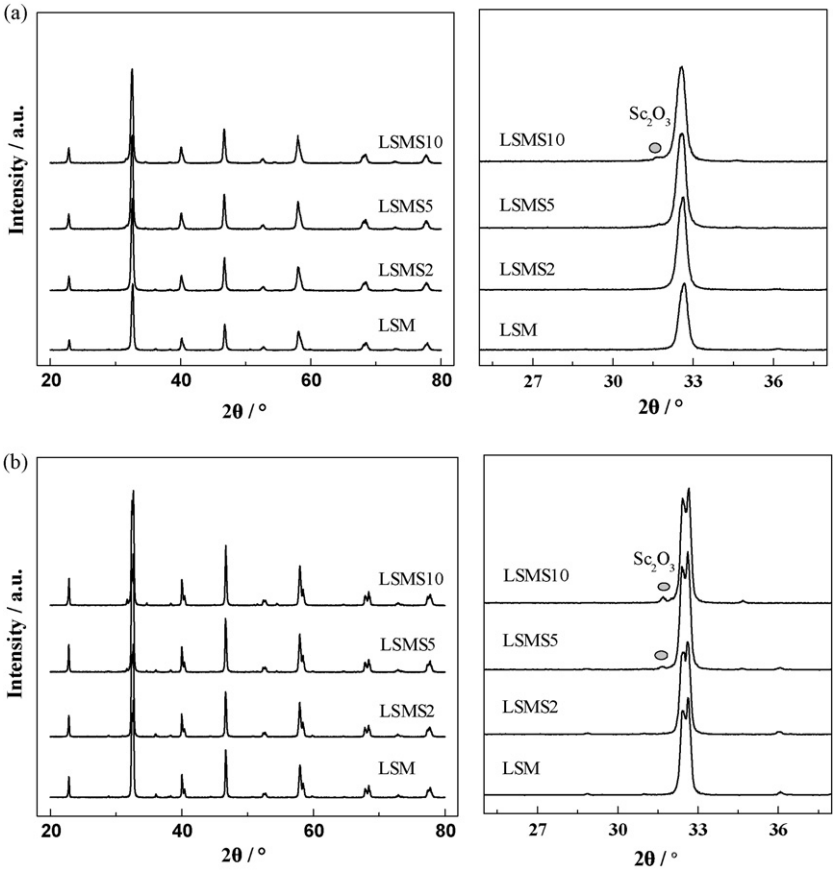

Fig. 1. XRD patterns of $La_{0.8}Sr_{0.2}Mn_{1-x}Sc_xO_{3\pm\delta}$ (LSMS) samples as a function of Sc content sintered at (a) 900 °C and (b) 1100 °C for 3 h. The magnified XRD pattern of the powders fired at both temperatures are also showed, the magnified range is 25–38°.

of substitution-induced non-stoichiometric defects into the perovskite lattice. As has also been reported by Lybye et al. [16,17], the scandium, as a large B-site dopant, is expected to expand the lattice and create more space for oxygen ion to travel through the lattice.

3.2. H_2-TPR investigation

H_2-TPR is an effective way to investigate the reducibility of metal ion and the mobility and availability of oxygen species [24]. The reduction profiles of the LSM along with its scandium-substituted homologues are presented in Fig. 2. The reduction profiles of LSM show two clear reduction stages, the first at 300–650 °C and the second at 700–850 °C. According to the literature [11,20,21,25], the low temperature reduction refers to the reduction of Mn (IV) to Mn (III), and the high temperature one relates to the reduction of Mn (III) to Mn(II), which leads to the breakdown of the perovskite structure. As can be seen in Fig. 2a and b, the position of the peaks representing both reduction processes depends on the calcination temperature. With the increase of temperature, the positions of the peaks consistently shift to higher temperatures, in agreement with the sintering processes.

Table 1
Positions of the strongest peaks, *d* values and average particle sizes of the LSMS samples prepared by modified Pechini method and sintered at different temperatures

Sintering temperature (°C)	Sample	2θ (°)	*d* (Å)	*D* (Å)[a]
900	LSM	32.660	2.7395	226
	LSMS2	32.639	2.7413	217
	LSMS5	32.580	2.7461	218
	LSMS10	32.580	2.7461	213
1100	LSM	32.621	2.7427	295
	LSMS2	32.601	2.7444	287
	LSMS5	32.601	2.7443	309
	LSMS10	32.659	2.7397	344

[a] The average particle sizes are determined without correction of instrumental broadening.

In the H_2-TPR profiles of LSMS samples, there are two reduction peaks similar to those of LSM counterpart. Since only Mn is reducible in LSMS, attributions of both peaks can be employed as the same with LSM. The peaks depicting the reduction of Mn (III), with slightly higher summit temperatures than LSM, are almost unchanged in position and shape. While the peak representing the reduction of Mn (IV) is increasingly shift to lower temperature with Sc concentration. For instance, the summit temperature of low temperature reduction for LSM, LSMS2, LSMS5, LSMS10 fired at 1050 °C (Fig. 2a) is 536, 526, 507, and 497 °C, respectively. It is quite interesting that the temperature downshift trends preserve when Sc_2O_3 phase forms at high degree of Sc doping (≥5 mol%). The decrease of reduction temperature with increasing Sc content is possibly due to the promotion of the fraction of Mn (IV) in the perovskite and the generation of oxygen vacancies which will facilitate the bulk diffusion and eventually accelerate the reduction, as have also been observed by other authors adopting different dopants [11,26]. For the samples calcined at 1100 °C (Fig. 2b), the summit temperatures reflecting the reduction of Mn (IV) for LSMS10 is the same with that of LSMS5, possibly because of the significant amount of Sc_2O_3 impurity, which might decline the surface area and give rise to a displacement of higher temperature of the reduction peaks.

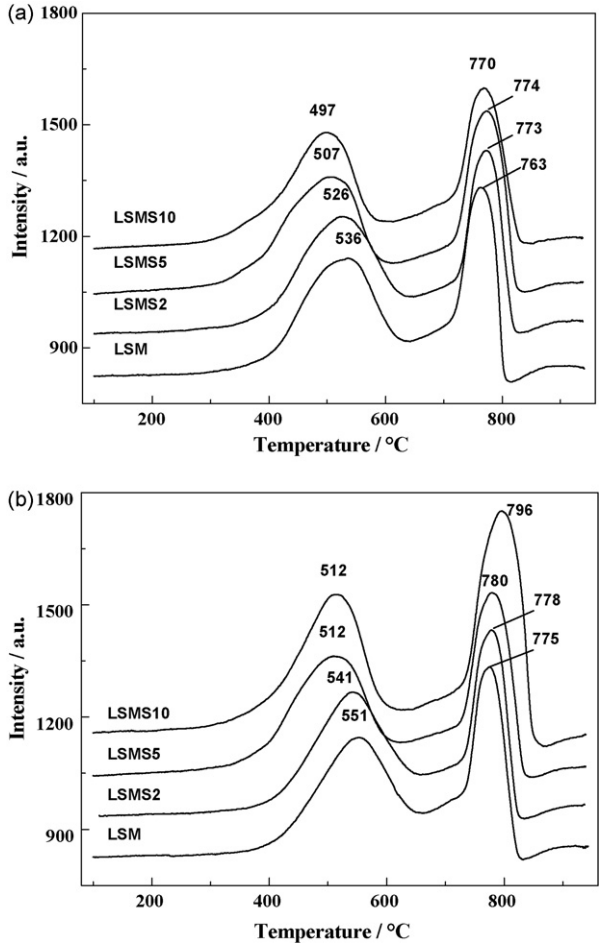

Fig. 2. H_2-TPR profiles of $LSMS_x$ samples sintered at (a) 1050 °C and (b) 1100 °C.

Through the H_2-TPR measurement, it can be obtained that the doping of Sc improves the low-temperature-reducibility of the LSMS samples. The precipitation of Sc_2O_3 possibly leads to cationic and oxygen anionic vacancies in the lattice, and the oxidation of Mn (III) to Mn (IV) to maintain the electrical neutrality, which may be the reasons for the increased reducibility for LSMS5 and LSMS10 samples. Meanwhile, the improved reducibility may be balanced by the significant amount of Sc_2O_3 impurity at higher sintering temperature as in the case of LSMS10 sample.

Ullamnn and Trofimenko [23] reported that the increased reducibility could be correlated with high oxygen ion mobility, therefore, it can be inferred that the high reducibility of LSMS samples is associated with high concentration of oxygen vacancies through which the oxygen ionic migrations take place [19,27]. Accordingly, it is reasonably presumed that a certain degree of Sc doping will positively affect the performance of LSM cathode considering the great importance of oxygen vacancies for this kind of material for IT-SOFC.

3.3. Cell performances and impedance analysis

Fig. 3 displays the *I–V* curves and the corresponding power densities of single cells with different composite cathodes measured at different temperatures. As has been expected in H_2-TPR discussions, the cell performance is greatly enhanced with low concentration of Sc doping into LSM in the composite cathode. The maximum power density (MPD) at 800 °C is 1.11, 1.44, and 1.30 W cm^{-2} for the cell with LSM–YSZ, LSMS2–YSZ, LSMS5–YSZ composite cathode, respectively. However, the MPD for the cell with LSMS10–YSZ composite cathode at 800 °C is slightly lower than that of the cell with LSM–YSZ composite cathode, which indicates that the further increase of Sc content brings adverse factors to the cell performance.

The performance improvement for LSMS2–YSZ, LSMS5–YSZ composite cathodes becomes impressively apparent at lower temperature. At 650 °C, for example, the cell with LSM–YSZ, LSMS2–YSZ, LSMS5–YSZ and LSMS10–YSZ composite cathode reaches the MPD of 0.18, 0.38, 0.39, and 0.23 W cm^{-2}, respectively. The cell with LSMS10–YSZ composite cathode exhibits a higher MPD than the cell with LSM–YSZ composite cathode at 650 °C, though it shows a slightly lower MPD than the latter at 800 °C. The above results make it clear that the partial substitution of Sc improves the cell performance at lower operating temperatures and excessive degree of doping (10 mol%) is unfavorable for further promotion of cell performance.

EIS is a useful tool to analyze the electrode kinetics and can provides information about the R_{ohm} and R_p from the rate determining steps in overall electrochemical processes. Fig. 4 displays the impedance spectra of single cells with different composite cathodes measured at different temperatures. Since the polarization from O_2 reduction is predominant on the anode supported SOFC, the impedance spectra mainly reflect the contributions from the cathodes [2–4]. In our study, all of the anode-electrolyte assemblies were nominally identical in respect that they were fabricated under the same conditions. Hereby, the discrepancies of the impedance behavior of distinct cells are mainly derived from the difference of the cathodes.

The Nyquist plots in Fig. 4 show two distinct arcs, except for the cell with LSM–YSZ composite cathode which shows an enlarged dominant arc at low frequency range below 750 °C. The arc located in the high frequency range is associated with the transport of oxygen ions and/or oxygen intermediates across LSMS/YSZ interfaces in addition to the transport through the YSZ phase in the composite [28,29]. The other arc lies in the low frequency range is correlated with the processes of dissociative adsorption of oxygen and diffusion of oxygen intermediates and/or oxygen anions on $LSMS_x$ surfaces and transfer of these species at TPBs [28–30]. At higher temperature (≥750 °C), the high frequency arcs for LSMS–YSZ composite cathode are depressed compared with that of LSM–YSZ composite cathode; the low frequency arc is minor in magnitude for LSMS2–YSZ and LSMS5–YSZ composite cathode, while it is comparable in magnitude for LSMS10–YSZ with LSM–YSZ composite cathode. Since the low frequency arc is strongly related to the length of TPBs [28], the increase in magnitude of the low frequency arc for LSMS10–YSZ composite cathode is assigned to the contamination to the TPBs resulted from the formation of large amount of Sc_2O_3 impurity. At lower temperature (≤700 °C), both arcs are drastically depressed for LSMS–YSZ cathode, in contrast with those of Sc-free cathode.

In Nyquist plots, the high frequency intercept with the real axis represents the overall R_{ohm} from the electrolyte, the electrodes, the interfaces of electrode/electrolyte and the leads. The low frequency intercept with the real axis reflects the total resistance of the cell under open circuit condition. The difference of the two intercepts corresponds to the polarization resistance, R_p. The correlations of R_{ohm}, R_p and the cell MPD with the concentration of Sc in corresponding cathode materials at 800 and 650 °C are shown in Fig. 5. It can be observed that the R_{ohm} decreases slightly when LSMS2–YSZ composite cathode is used, possibly because the low concentration of Sc in perovskite improves the ion conduction without producing Sc_2O_3 impurity concurrently. On the contrary, R_{ohm} increases apparently for the cathodes with further more content of Sc. This can be interpreted by the fact that Sc_2O_3

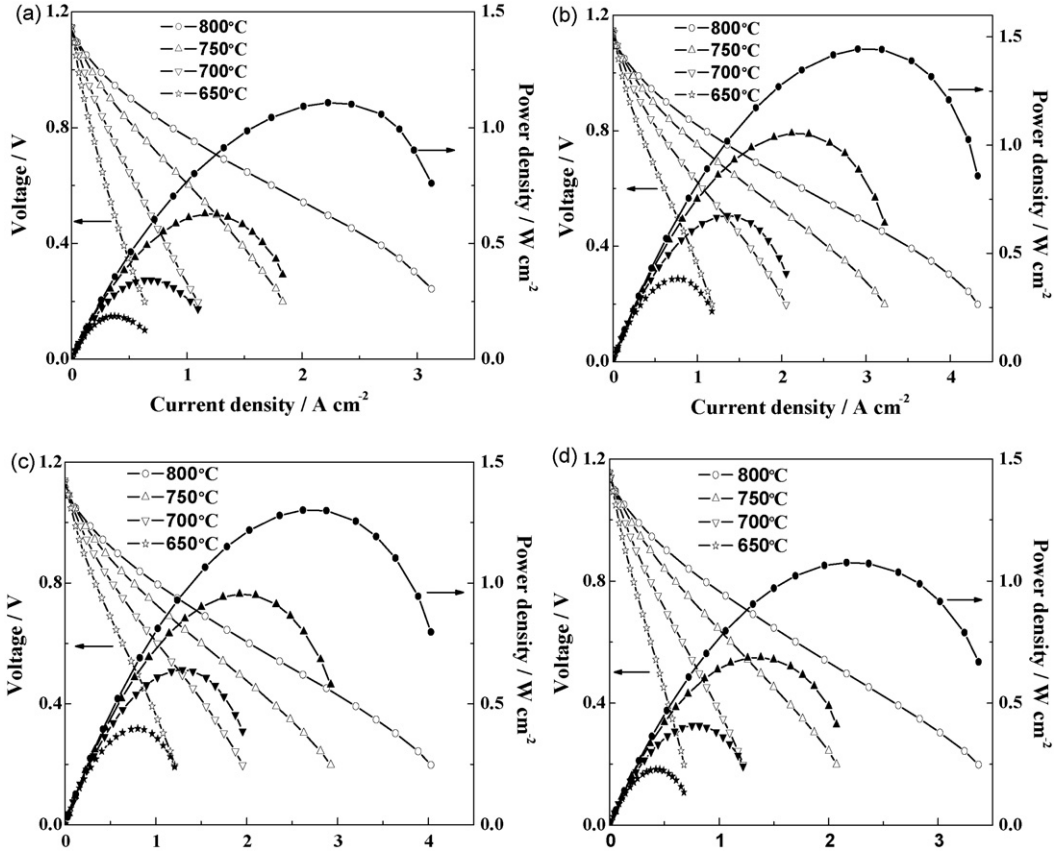

Fig. 3. Voltage and power density vs. current density for the single cells with different composite cathodes: (a) LSM–YSZ, (b) LSMS2–YSZ, (c) LSMS5–YSZ and (d) LSMS10–YSZ.

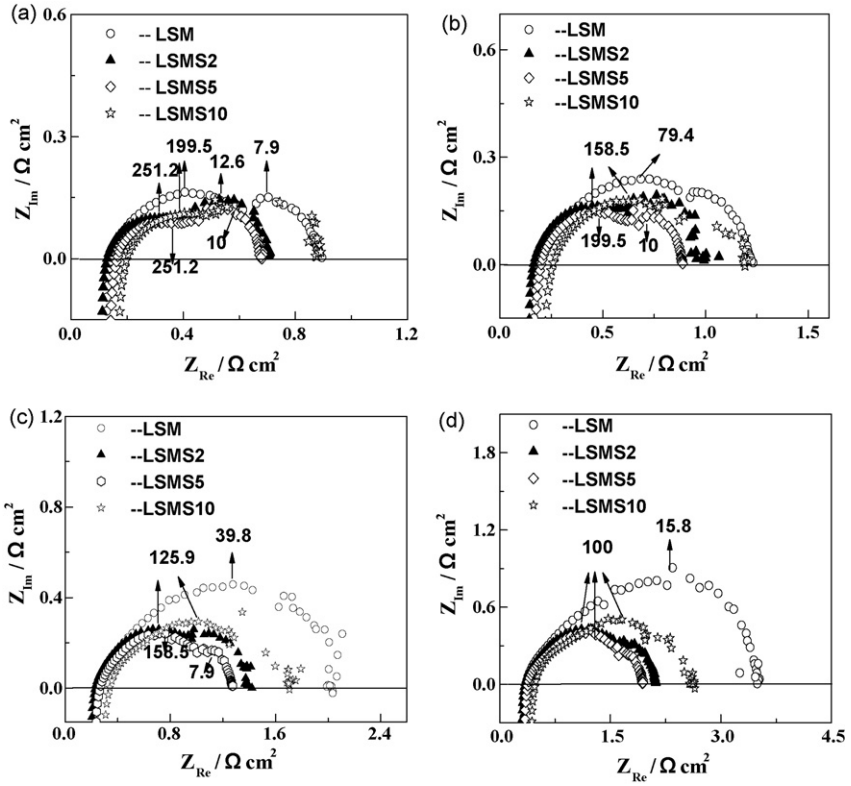

Fig. 4. Nyquist plots of single cells with different composite cathodes measured at (a) 800 °C, (b) 750 °C, (c) 700 °C and (d) 650 °C. The summit frequencies of the corresponding arcs are interposed.

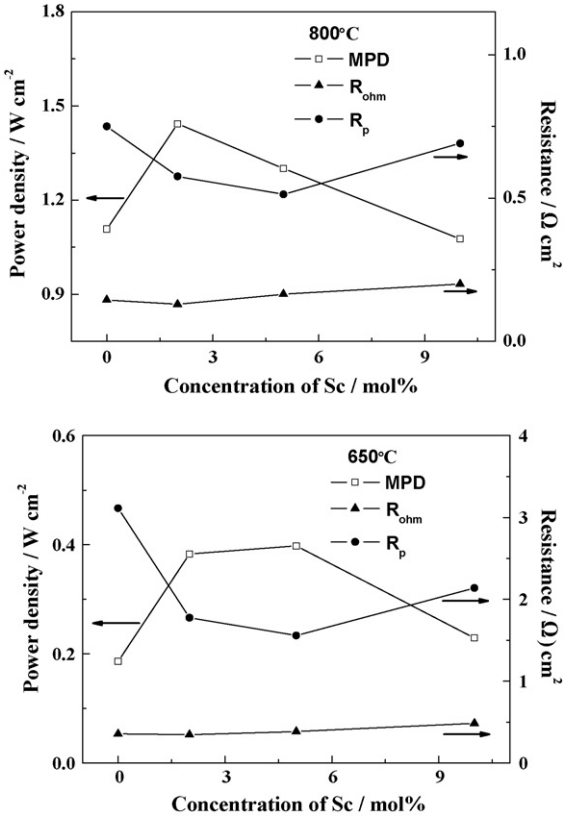

Fig. 5. Maximum power density (MPD), ohmic resistance (R_{ohm}) and polarization resistances (R_p) of single cells with different Sc content in the LSMS–YSZ composite cathodes at 800 and 650 °C.

impurities tend to precipitate with the rising of Sc content, thus form an insulate phase at the cathode/electrolyte interface, which becomes a prime factor for the increase of R_{ohm}.

With respect to R_p, with the increase of Sc concentration, R_p decreases first, attains the minimum for the cell with LSMS5–YSZ composite cathode and then increases. At 800 °C, for the cell with LSMS2–YSZ, LSMS5–YSZ, LSMS10–YSZ composite cathode, the R_p is 76%, 68%, and 92% of that of the cell with LSM–YSZ composite cathode, respectively. What is impressive is that, all the cells with LSMS–YSZ composite cathode show much lower R_p than that of the cell with LSM–YSZ composite cathode at 650 °C, rationally revealing the reason for the performance enhancement for LSMS-based cathode as R_p plays a dominant role for the cell performance at reduced temperature range.

It has been tentatively concluded in TPR analysis that the concentration of oxygen anionic vacancies increased considerably as a result of incorporation of Sc into LSM perovskite lattice. As has been verified by many researchers, oxygen vacancies play a tremendous role in the electrochemical processes occurred in the SOFC cathode side [14,15,31]. The LSM–YSZ composite cathode, showing increasingly higher R_p with reducing temperature, is considered to suffer from the absence of sufficient oxygen vacancies [6–9], thus the retarded electrode kinetics and inferior MPD. In comparison, a certain degree of Sc-doped LSMS-based composite cathodes profit from the increase of substitution-generated oxygen vacancies, in line with the supposition from TPR results. Consequently, it can rationally conclude that the introducing of Sc into LSM perovskite accelerates the rate-determining electrochemical processes occurred in LSM-based cathode (Fig. 4), and Sc-doped LSMS materials show higher electrochemical activity towards oxygen reduction reaction than LSM cathode material, especially at lower operating temperature. Lastly, it is worth stressing that excessive degree of doping introduces impurity to the cathode, hence causes the decrease of the cell performance. In this work (Fig. 5), the MPD of the cell with LSMS10–YSZ cathode is lower than the cells with low degree of substitution in LSM in the composite cathode.

4. Conclusions

$La_{0.8}Sr_{0.2}Mn_{1-x}Sc_xO_{3-\delta}$ samples with $x = 0$, 2, 5, and 10 mol% are prepared using modified Pechini method. The XRD results indicate that Sc_2O_3 tends to segregate from the perovskite phase at Sc concentration higher than 5 mol%. The TPR results depict that the reducibility of LSM-based materials is greatly improved due to the substitution of Sc, which promotes the fraction of Mn (IV) and oxygen vacancies. However, the reducibility may be balanced by the appearance Sc_2O_3 impurity for the sample with high degree of doping at elevated firing temperature. The performance evaluations for the cells with LSMS–YSZ cathodes show that at higher operating temperature, minor amount of Sc substitution is beneficial, whereas high concentration of Sc, about 10 mol% in this work, reduces the cell performance mainly because Sc_2O_3 impurities increases the R_{ohm}. At lower operating temperature, all the cells with the LSMS–YSZ composite cathodes show higher performance than the one with the LSM–YSZ composite cathode, which can mainly originate from the increase of oxygen anionic vacancies for the LSMS, suggesting that the incorporation of Sc in LSM brings improved electrochemical activity towards O_2 reduction reaction.

Acknowledgments

The authors gratefully acknowledge financial supports from the Ministry of Science and Technology of China (No. 2004CB719506, 2005CB221404 and 2006AA05Z147) and National Natural Science Foundation of China (No. 20676132).

References

[1] B.C.H. Steele, A. Heinzel, Nature 414 (2001) 345–352.
[2] T. Tsai, S.A. Barnett, Solid State Ionics 93 (1997) 207–217.
[3] M.J.L. Østergard, C. Clausen, C. Bagger, M. Mogensen, Electrochim. Acta 40 (1994) 1971–1981.
[4] E.P. Murray, T. Tsai, S.A. Barnett, Solid State Ionics 110 (1998) 235–243.
[5] V.A.C. Haanappel, J. Mertens, D. Rutenbeck, C. Tropartz, W. Herzhof, D. Sebold, F. Tietz, J. Power Sources 141 (2005) 216–226.
[6] T.L. Reitz, H. Xiao, J. Power Sources 161 (2006) 437–443.
[7] V.A.C. Haanappel, A. Mai, J. Mertens, Solid State Ionics 177 (2006) 2033–2037.
[8] E.P. Murray, S.A. Barnett, Solid State Ionics 143 (2001) 265–273.
[9] M. Zhang, M. Yang, B. Liu, Z. Hou, Y. Dong, M. Cheng, J. Power Sources 175 (2008) 739–748.
[10] S.P. Jiang, Solid State Ionics 146 (2002) 1–22.
[11] M.R. Pai, B.N. Wani, B. Sreedhar, S. Singh, N.M. Gupta, J. Mol. Catal. A: Chem. 246 (2006) 128–135.
[12] S. Carter, A. Selcuk, R.J. Chater, J. Kajda, J.A. Kilner, B.C.H. Steele, Solid State Ionics 53–56 (1992) 597–605.
[13] P. Porta, S. De Rossi, M. Faticanti, G. Minelli, I. Pettiti, L. Lisi, M. Turco, J. Solid State Chem. 146 (1999) 291–304.
[14] R.A. De Souza, J.A. Kilner, Solid State Ionics 106 (1998) 175–187.
[15] R.A. De Souza, J.A. Kilner, Solid State Ionics 126 (1999) 153–161.
[16] D. Lybye, N. Bonanos, Solid State Ionics 125 (1999) 339–344.
[17] D. Lybye, F. Poulsen, M. Mogensen, Solid State Ionics 128 (2000) 91–103.
[18] K. Nomura, T. Takeuchi, S. Tanase, H. Kageyama, K. Tanimoto, Y. Miyazaki, Solid State Ionics 154–155 (2002) 647–652.
[19] M.A. Peña, J.L. Fierro, Chem. Rev. 101 (2001) 1981–2017.
[20] S. Cimino, S. Colonna, S. De Rossi, M. Faticanti, L. Lisi, I. Pettiti, P. Porta, J. Catal. 205 (2002) 309–317.
[21] L. Lisi, G. Bagnasco, P. Ciambelli, S. De Rossi, P. Porta, G. Russo, M. Turco, J. Solid State Chem. 146 (1999) 176–183.
[22] H. Yokokawa, N. Sakai, T. Kawada, M. Dokiya, Solid State Ionics 52 (1992) 43–56.
[23] H. Ullmann, N. Trofimenko, Solid State Ionics 119 (1999) 1–8.

[24] R. Bell, G. Millar, J. Drennan, Solid State Ionics 131 (2000) 211–220.
[25] P. Ciambelli, S. Cimino, S. De Rossi, M. Faticanti, L. Lisi, G. Minelli, I. Pettiti, P. Porta, G. Russo, M. Turco, Appl. Catal. B: Environ. 24 (2000) 243–253.
[26] W. Wang, H. Zhang, G. Lin, Z. Xiong, Appl. Catal. B: Environ. 24 (2000) 219–232.
[27] Y. Ji, J.A. Kilner, M.F. Carolan, Solid State Ionics 176 (2005) 937–943.
[28] M.J.L. Østergard, M. Mogensen, Electrochim. Acta 38 (1993) 2015–2020.
[29] S.P. Jiang, J.G. Love, Y. Ramprakash, J. Power Sources 110 (2002) 201–208.
[30] M.J. Jørgensen, M. Mogensen, J. Electrochem. Soc. 148 (2001) A433–A442.
[31] S. Adler, J.A. Lane, B.C.H. Steele, J. Electrochem. Soc. 143 (1996) 3554–3564.